RSC Advances

ROYAL SOCIETY OF CHEMISTRY

www.rsc.org/advances

Biomimetic Setaria Viridis-Inspired Imprinted Nanoadsorbent: Green Synthesis and Application for Highly Selective and Fast Removal of Sulfamethazine

Ping Ma[1], Zhiping Zhou[1,*], Jiangdong Dai[1,2], Ling Qin[1], Xubo Ye[1], Xiang Chen[2], Jinsong He[2], Atian Xie[2], Yongsheng Yan[2], Chunxiang Li[2,*]

[1] School of Material Science and Engineering, Jiangsu University, Zhenjiang 212013, China

[2] School of Chemistry and Chemical Engineering, Jiangsu University, Zhenjiang 212013, China

Abstract

Nowadays, it is very necessary to develop high-efficiency nanoadsorbents to remove drug contaminants from wastewater. Inspired by biomimetic setaria viridis-like structure, we provided a simple and general approach for the preparation of hydrophilic magnetic surface molecularly imprinted core-shell nanorods (HMMINs), *via* a two-step surface-initiated atom transfer radical polymerization in a green alcohol/water mixture solvent at room temperature, with magnetic halloysite nanotubes (HNTs, a hollow tubular structured natural clay mineral) used as nano-cores. HMMINs showed a well-defined core-shell structure with ultrathin imprinted film (12 nm) and hydrophilic polymer brushes (2-4 nm), where magnetic nanoparticles (11 nm) were uniformly dispersed onto surface of halloysite nanotubes. HMMINs possessed the good magnetic property and thermal stability. Surface grafting of hydrophilic polymer brushes enhanced adsorption selectivity and kinetics rate. HMMINs exhibited a large adsorption capacity (37.64±1.36 μmol g^{-1}) and fast kinetics (within 45 min) toward a typical antibiotic drug sulfamethazine (SMZ) from pure water. Adsorption isotherm and kinetics data was well described by Freundlich isotherm model and psedo-second-order kinetic equation, respectively. HMMINs displayed the good selectivity toward SMZ as compared with other antibiotics, as well as regeneration performance, providing a potentially practical application in the highly efficient and selective removal of antibiotic contaminants from wastewater.

Keywords: Biomimetic setaria viridis-inspired structure; Selective sulfamethazine removal; Water-phase synthesis; Ultrathin hydrophilic imprinted nanofilm; Magnetic halloysite nanotubes

∗ Corresponding author. Tel.: +86-0511-88790683; fax: +86-0511-88791800.

E-mail address: Zhouzp@ujs.edu.cn (Z.P. Zhou); ujs2013txh@163.com (C.X. Li)

1. Introduction

The widespread occurrence of veterinary antibiotics detected in food and eco-environments, particularly in the aquatic systems, has remarkably attracted more and more international concerns [1, 2]. Sulfonamides (SAs), as a class of bacteriostatic agents, are the most commonly used to treat humans and animals and/or to promote growth in animals for more than sixty years, due to their broad-spectrum activity against infections caused by gram-positive and gram-negative bacteria and relatively low cost. However, a high proportion of unmetabolized SAs are excreted in parent forms and finally transported from manured field to water environments. The intake of SAs (particularly sulfamethazine, SMZ) through food chains and drinking water into body is dangerous for human health, which can cause adverse effects including allergic reactions, disbacteriosis and even carcinogenic effects [3, 4]. Conventional water treatment methods, such as coagulation, flocculation, sedimentation and ion exchange, are relatively ineffective in removing antibiotic pollutions from wastewater. Due to its relatively low cost and high efficiency, adsorption is usually considered as an effective method to eliminate many organic pollutants [5-7]. Adsorption performance of the used adsorbents is key to remove targeted substance. Thus, it is very important to synthesize novel and high-performance adsorbents to remove SAs from water environments.

Molecularly imprinting, as an advanced and powerful technique, can make aritifical receptors with the strong ability to recognize and rebind predetermined/targeted molecules [8]. Due to their excellent characteristics, such as easy preparation, specific recognition, low cost and high stability, molecularly imprinted polymers (MIPs) have attracted more and more attention in a wide range of application fields including solid phase extraction, chromatography, sensor, catalysis and so on [9-12]. However, conventional bulk MIPs prepared by traditional techniques, owing to the highly cross-linked nature, suffer from many limitations, such as time-consuming crush, heterogeneous particle size, difficult template removal and low adsorption/desorption kinetics, thereby decreasing the rebinding efficiency. Thus, the development of high-efficient imprinted techniques to solve these problems is notably important. The establishment of nanoimprinted system is an effective approach, which controls template molecules to be located in the surface or approximate surface, namely surface imprinted technique [13-15]. The preparation of core-shell MIPs has recently provided a general method for obtaining surface imprinted polymers with various solids as core

materials.

Halloysite nanotubes (HNTs, $Al_2Si_2O_5(OH)_4 \cdot nH_2O$) are 1:1 layer silicate clay minerals with an obvious hollow tubular structure, where the outer surface and the inner surface consists of a tetrahedral (Si-O) and an octahedral (Al-OH) sheet, respectively [16, 17]. The chemical properties of HNTs are similar with pure SiO_2 and Al_2O_3. Generally, the size range of the inner and outer diameters for HNTs is 10-30 nm and 50-100 nm, respectively. Owing to superior characteristics including high porosity, large surface area and tunable surface chemistry, HNTs have attracted great interest in chemical, material and environmental science, especially for catalysis, drug delivery, template and separation [18-21]. Compared with the artificial synthetic materials (e.g. carbon nanotubes, silica-based materials and polymer spheres), HNTs are cheaper and surface hydrophilic, and thus can be used an ideal core material for loading imprinted polymers. In our previous research, magnetic nanoparticles were first loaded onto HNTs, and the imprinted polymer nanoshell with a tunable thickness was coated onto the HNTs' surface *via* a simple precipitation polymerization [22]. When magnetic property is introduced into molecularly imprinted polymers, the obtained imprinted composites can be easily collected in the present of an external magnetic field and facilitate separation process.

Usually, the preparation and application of MIPs are mostly restricted in various organic solvents, but natural recognition system and practical applications for MIPs are mainly in the water environments. Obviously, it is necessary to develop novel hydrophilic MIPs, which can be applied in water-phase systems. Two strategies have been developed to improve the MIPs' surface hydrophilicity. One involves the copolymerization of hydrophilic monomer, functional monomer and cross-linking agent in the synthesis process [23-25]. Although the process is very simple, the optimization of synthesis parameters is complicated and time-consuming, which can affect MIPs' properties due to the extra addition of hydrophilic monomers. Another way is post-modification of the already obtained imprinted materials [26-28], which is relatively simple and low-cost. Also, the persistent pursuit of general and facile methodologies was highly desirable to develop hydrophilic MIPs.

Atom transfer radical polymerization (ATRP), as a new class of controllable radical technique, has been recently used for the generation of MIPs to improve their properties in the

field of molecular imprinting [29-32]. ATRP is tolerant of a wide range of polymerable monomers and can be carried out in the mild reaction conditions, such as low temperature (especially at room temperature) and water-phase environments [33, 34]. Previously, we reported that narrowly dispersed imprinted microspheres were first prepared by reverse ATRP and then used as macro-active initiator for further surface-modification of hydrophilic polymer brushes [35]. It is proved that ATRP is a powerful technique to synthesize the "living" polymers with well-defined structures, which can be used as macro-initiator for further surface multi-functionalization.

To the best of our knowledge, the preparation of hydrophilic magnetic organic-inorganic selective nanoadsorbents and their application in the selective recognition and removal of sulfamethazine antibiotic in pure water was reported herein for the first time. Biomimetic inspired by the unique appearance of a common green plant, setaria viridis, which has a rod-like tassel with abundant bristles structure along the plant stem (as shown in Fig. 1)[36]. The aim of this work is to prepare the hydrophilic magnetic surface molecularly imprinting core-shell nanorods (HMMINs) based onto magnetic halloysite nanotubes, *via* a facile two-step ATRP in a green alcohol/water mixture solvent at room temperature. The obtained HMMINs were used to adsorption and remove the SMZ antibiotic from water environments. The physical and chemical properties, adsorption isotherms, adsorption kinetics, selectivity and regeneration performance of HMMINs towards SMZ were investigated in detail through batch adsorption technique.

2. Experimental

2.1. Materials

HNTs were purchased from Zhengzhou Jinyangguang Chinaware Co., Ltd, Henan, China and were purified by repeated sedimentation processes to remove the quartz impurities, followed by drying at 80 °C for 12 h and grinding. 4-vinylpyridine (4-VP, 96%), hydroxyethyl methylacrylate (HEMA, 96%), 2-bromoisobutyryl bromide (2-BiBr, 98%), 3-aminopropyltriethoxysilane (APTES, 99%), N,N,N',N",N"-Pentamethyldiethylenetriamine (PMDETA, 98%), SMZ (98%), tetracycline (TC, 98%), ethylene glycol dimethacrylate (EGDMA, 98%) and ciprofloxacin (CIP, 98%) were analytical reagents and were purchased from Aladdin Reagent Co., Ltd. (Shanghai, China). Cuprous bromide (CuBr), anhydrous toluene, acetone, acetic acid, ethanol, methanol, ethylene glycol (EG, 98%), iron (III) nitrate nonahydrate ($Fe(NO_3)_3 \cdot 9H_2O$, 98%), dichloromethane and

triethylamine were analytical reagents and were purchased from Sinopharm Chemical Reagent Co. Ltd. (Shanghai, China). Deionized ultrapure water was obtained from a Purelab Ultra system (Organo, Tokyo, Japan).

2.2. Preparation of magnetic halloysite nanotubes (MHNTs)

5.0 g of HNTs were added into 150 ml of HNO_3 aqueous solution (2.0 mol L^{-1}) in a three neck flask and uniformly dispersed under ultrasound for 30 min. The mixtures were vigorously stirred to remove the impurities at 80 ^oC for 12 h. The resultant product was collected by vacuum filtration, was repeatedly washed with deionized water and was dried in oven. Subsequently, 1.0 g of HNTs and 0.6 g of $Fe(NO_3)_3 \cdot 9H_2O$ were added into 20 ml of ethanol under ultrasound for complete dispersion and dissolution. After stirring at room temperature overnight, the mixture were dried at 60 ^oC until ethanol was completely evaporated. The yellow solid was impregnated with 2.0 ml of EG and heated at 400 °C for 2.0 h with a heating rate of 5.0 °C min^{-1} under the protection of nitrogen in a tube furnace. The black product was repeatedly washed with ethanol and water, and dried to obtain MHNTs.

2.3. Preparation of -NH_2 modified MHNTs (MHNTs@NH_2)

1.0 g of MHNTs were added into 100 ml of anhydrous toluene in a three neck flask (250 ml) and uniformly dispersed under ultrasound. 1.5 ml of APTES was added and the mixture was vigorously stirred and reacted at 90 ^oC for 24 h. After reaction, the product was collected with the help of an external magnet, and was alternately washed with ethanol and deionized water for several times, following by drying to constant weight. The APTES modified was obtained and denoted as MHNTs@NH_2.

2.4. Preparation of "living" -Br modified MHNTs (MHNTs@Br)

0.5 g of MHNTs@NH_2 and 50 ml of dichloromethane were added into a round bottom flask, and were uniformly dispersed under ultrasound. Then 1.0 ml of triethylamine and 1.0 ml of 2-bromoisobutyryl bromide were added to the mixture solution. Under the nitrogen protection, the reaction was carried out at 0 ^oC for 2.0 h and at 25 ^oC for 12 h with vigorous agitration. After complete reaction, the resultant product was washed with water and ethanol, and was dried to constant weight. The "living" -Br modified MHNTs was denoted MHNTs@Br.

2.5. Preparation of magnetic surface molecularly imprinting core-shell nanorods (MMINs)

In the synthesis process of imprinted nanoadsorbent, SMZ was used as the template molecule, 4-VP as the functional monomer, and EGDMA as the cross-linking agent. 16 ml of methanol and 4.0 ml of water were added into a flask. 27.8 mg of SMZ, 0.26 ml of 4-VP and 2.30 ml of EGDMA were added to the solvent and self-assembled for 12 h at room temperature in dark. Under nitrogen protection, 14.3 mg of CuBr and 42.3 μl of PMDETA were added. 0.2 g of MHNTs@Br were finally added to the mixture solution. The reaction was performed 25 ^{o}C for 24 h with vigorous stirring. After reaction, the product was washed with ethanol and acetone for six times, and was dried in 60 ^{o}C for 12 h. The template molecules was removed from the obtained product through soxhlet extraction using the mixture of methanol and acetic acid (9.0:1.0, v:v) as eluent until SMZ could not be detected. Magnetic surface molecularly imprinting core-shell nanorods (MMINs) was obtained. For comparsion, by the same method, magnetic surface non-imprinting core-shell nanorods (MNINs) was also prepared without the addition of template molecules in the polymerization process.

2.6. Preparation of hydrophilic magnetic surface molecularly imprinting core-shell nanorods (HMMINs)

In brief, 2.0 ml of deionized water and 2.0 ml of methanol were added into a 25 ml of flask. 10.47 mg of CuBr, 45.8 μl of PMEDTA and 1.5 ml of HEMA were added to form a homogeneous solution. Then the solution was degassed under ultrasound and exchanged with N_2 to remove oxygen. 100 mg of MMINs were added into the flask and the reaction was carried out at 25 ^{o}C for 24 h. The product was washed with acetone, ethanol and water for six times, and then was dried in oven to obtain HMMINs. The hydrophilic magnetic surface molecularly non-imprinting core-shell nanorods (HMNINs) were prepared by the same method, just with the addition of MNINs as macro-initiator.

2.7. Batch adsorption experiments

Adsorption isotherm experiments were performed to study adsorption equilibrium property of these nanoadsorbents. 5.0 mg of MMINs, HMMINs, MNINs and HMNINs were added to SMZ aqueous solutions with the different initial concentrations between 5.0 and 120 μmol L^{-1}. The adsorption experiments were carried out 25 ^{o}C for 12 h to reach equilibrium. The adsorbents were quickly separated with the help of an external magnet. Free SMZ concentrations in solutions were

measured by UV-vis spectrophotometer (UV-2450, Shimadzu, Japan) at 249 nm. The equilibrium adsorption capacities Q_e (μmol g^{-1}) of SMZ were calculated according to the following equation:

$$Q_e = \frac{(C_o - C_e)V}{m} \quad (1)$$

where C_o and C_e (μmol L^{-1}) are the initial and equilibrium SMZ concentration, respectively. V (L) and m (g) are volume of solution and mass of nanoadsorbent, respectively.

To investigate adsorption kinetic property of nanoadsorbents, 5.0 mg of MMINs, HMMINs, MNINs and HMNINs were added into 10 ml of SMZ solution with the initial concentration of 100 μmol L^{-1}, respectively. The adsorption experiments were conducted at 25 ^oC for the different contact time, including 10, 20, 30, 45, 60, 90 and 120 min, respectively. The supernatant was quickly obtained with the help of an external magnet and was then tested. The adsorption amounts of SMZ (Q_t, μmol g^{-1}) at time t (min) were calculated according to the following equation:

$$Q_t = \frac{V(C_o - C_t)}{m} \quad (2)$$

where C_t (μmol L^{-1}) is the free SMZ concentration at any time t.

The selective recognition property of HMMINs was studied by adsorption experiments using TC and CIP as reference antibiotics. 5.0 mg of HMMINs and HMNINs were added to each antibiotic solution with the initial concentration of 100 μmol L^{-1}, respectively. After adsorption reached equilibrium at 25 ^oC, nanoadsorbents were separated under an external magnetic field, and the free antibiotic concentrations of TC and CIP were tested by UV-vis spectrophotometer at 357 nm and 276 nm, respectively.

All the adsorption experiments were carried out by six times, and the experimental data was stable and reproducible, the error of which was much less than 5.0 %.

2.8. Instruments

Fourier Transform infrared spectroscopy was recorded on a Nicolet NEXUS-470 FTIR apparatus (U.S.A.) using KBr pellet technique. Scanning electron microscopy (SEM, S-4800, Hitachi, Japan) and transmission electron microscope (TEM, JEOL IEM-200CX, U.S.A) were used to describe the morphology of samples. Magnetic measurement was carried out using a VSM (7300, Lakeshore, U.S.A) under a magnetic field up to 10 kOe. Thermal gravimetric analysis (TGA) of samples was measured using a Diamond TG/DTA instruments (STA 449C Jupiter,

Netzsch, Germany) under N_2 up to 800 ^oC with a heating rate of 10 ^oC min^{-1}. Samples were dispersed into in ethanol under ultrasound (20 mg mL^{-1}), and dropped onto clean glass, respectively. After the ethanol was allowed to be evaporated at ambient temperature, the static water contact angle was tested by a contact angle instrument (KSV CM200, Finland).

3. Results and discussion

3.1. Preparation method for HMMINs

Fig. 1 shows the schematic diagram of synthetic route for HMMINs. Firstly, the iron ions were introduced into the lumen and surface of HNTs through the wetness impregnation. MHNTs were obtained by the reduction of iron ions with EG at high temperature under the protection of nitrogen. Secondly, amino and bromine groups were successively modified onto the surface of MHNTs by silanization reaction and amidation reaction to obtain MHNTs@NH_2 and MHNTs@Br, respectively. Thirdly, magnetic surface molecularly imprinting core-shell nanorods (MMINs) were prepared by a surface-initiated ATRP at room temperature, using the mixture of methanol and water as the reaction solvent, SMZ as the template molecule, 4-VP as the functional monomer, EGDMA as the cross-linking agent, PMDETA and CuBr as catalyst system. Finally, poly(HEMA) (PHEMA) brushes were grafted from MMINs' surface via a surface-initiated ATRP method again, to obtain HMMINs with the selective recognition ability. This imprinted polymerization technique is non-toxic and low energy consumption, as compared with other previous methods for preparing hydrophilic MIPs [23-28].

3.2. Characterization

Fig. 2 shows FT-IR spectra of MHNTs, MHNTs@NH_2, MHNTs@Br, MMINs and HMMINs. As shown in the spectrum of MHNTs, the characteristic peaks at 1087 and 1032 cm^{-1} came from Si-O and Si-O-Si stretching vibrations, respectively. The sharp peaks at 3707 and 3622 cm^{-1} were attributed to stretching vibration of the inner surface -OH and deformation vibration of the inner surface -OH occurred at 912 cm^{-1}. Deformation vibration of Al-O-Si bond can be clearly observed at 534 cm^{-1} [37]. The peak intensity of Fe-O bond was too weak to be detected. The spectrum of MHNTs@NH_2 showed a weak peak at 2954 cm^{-1}, which was assigned to -CH_2 stretching vibration of APTES. The broad peak at 3452 cm^{-1} belonged to -NH_2 stretching vibration. After amidation reaction, the peak of amide carbonyl group was found at 1649 cm^{-1} in the spectrum of

MHNTs@Br, indicating that the initial group was successfully grafted onto the surface of MHNTs. In the spectra of MMINs, C=N characteristic peak in pyridine ring occurred at 1601 and 1558 cm^{-1}, and C=O stretching vibration was seen at 1725 cm^{-1}, demonstrating 4-VP and EGDMA were successfully grafted from MHNTs' surface. It could be seen that the intensity of peak at 1158 and 1245 cm^{-1} was enhanced, which came from the C-O-C stretching vibration. Meanwhile, -OH characteristic peak at 3435 cm^{-1} increased. Thus, PHEMA brushes were well introduced onto the MMINs' surface.

Fig. 3 shows SEM images of HNTs, MHNTs, MMINs and HMMINs. HNTs had a tubular structure with a length of 1.0-3.0 μm and an external diameter of 50-180 nm. As compared with HNTs, the overall morphology of MHNTs was not changed. MHNTs' surface became a little more rough, which might be caused by the load of magnetic nanoparticles. After grafting of imprinted polymers, both the length and diameter of MMINs increased slightly. In Fig. 3d, HMMINs had a smooth surface and a little cross-linking.

In order to further obtain their morphology and structure information, TEM was used to characterize HNTs, MHNTs, MMINs and HMMINs, as shown in Fig. 4. HNTs exhibited hollow a tubular structure with non-uniform length and diameter. From Fig. 4b, it could be clearly seen that magnetic nanoparticles were uniformly dispersed into the lumen and onto the surface of HNTs, and has an average size of 11 nm. In Fig. 3c, MMINs showed an evident core-shell structure, with imprinted polymer nanoshell thickness of about 12 nm. After surface grafting of PHEMA, the polymer nanoshell thickness increased to 14-16 nm, so the average thickness of polymer brushes was in the range of 2-4 nm. From the results of SEM and TEM images, the imprinted nanofilm and polymer brushes were successfully grafted onto the surface of MHNTs.

Fig. 5A represents magnetization curves of MHNTs, MMINs and HMMINs. It is obvious that three samples were all no hysteresis, and remanence and coercivity were near zero in hysteresis loop, suggesting the samples were superparamagnetic. Magnetization saturation (*M*s) value of MHNTs was 2.81±0.071 emu g^{-1} at 298 K. After surface grafting of imprinted polymer, *M*s value of MMINs reduced to 2.51±0.056 emu g^{-1}. Meanwhile, *M*s value of HMMINs was 2.29±0.042 emu g^{-1}. With the increase of polymer shell thickness, the *M*s value decreased gradually, which was well matched with the result of TEM images. Although the *M*s value of HMMINs was not

very large, it was enough to achieve magnetic separation. As shown in Fig. 5B, HMMINs was uniformly dispersed in pure water in a glass bottle. When a magnet was close to the bottle, HMMINs moved quickly to the wall of bottle, and the solution became clear soon. HMMINs showed a good separation performance in aqueous environment.

Fig. 6 shows TGA curves of MHNTs, MHNTs@NH_2, MHNTs@Br, MMINs and HMMINs. At temperature below 200 °C, only a low proportion of mass loss was observed for MHNTs, due to the evaporation of physically absorbed water. In the temperature range of 400-800 °C, because of dehydration of Al-OH group in the lattice, the mass loss ratio of MHNTs at 800 °C was 11.83%. After silanization reaction, the mass loss ratio of MHNTs@NH_2 was 14.52%. The mass loss of MHNTs@Br increased to 15.52%, indicating the initiator was grafted onto the surface by amidation reaction. For MMINs and HMMINs, the mass loss mainly occurred at a temperature range of 300-600 ^{o}C, due to the thermal decomposition of polymers. The mass loss ratios of MMINs and HMMINs were about 29.78 and 43.62%, respectively. As obviously described in the TGA curves, weight loss of the samples gradually increased step-by-step, which demonstrated that each reaction step was completed successfully.

Fig. 7 shows the photographs of static water contact angles for MMINs and HMMINs. It can be clearly seen that HMMINs showed much lower static water contact angle than MMINs. The static water contact angles of MMINs and HMMINs were 122.34±0.4 and 45.14±0.2^{o}, respectively, which indicated the PHEMA brushes were grafted successfully onto the surface of MMINs and improved the surface hydrophilicity.

3.3. Adsorption Isotherms

Fig. 8A shows adsorption isotherm curves of MMINs, MNINs, HMMINs and HMNINs towards SMZ at 298 K. In the whole concentration range, the adsorption amount increased with the increase of initial concentrations, and gradually reached the adsorption equilibrium. The adsorption capacities of MMINs and HMMINs were much higher than that of MNINs and HMNINs, indicating that the imprinted sites were existed in the polymer network. The adsorption capacities of SMZ onto MMINs, MNINs, HMMINs and HMNINs in aqueous solutions were 43.82±1.85, 20.18±0.625, 37.64±1.36 and 14.42±0.649 μmol g^{-1}, respectively. Here our obtained HMMINs nanoadsorbent showed a higher adsorption affinity to template SMZ than other reported

SMZ-imprinted adsorbents [38-41]. It is clearly observed that the adsorption amount decreased after surface grafting of hydrophilic polymer brushes in Fig. 8A, which could inhibit the hydrophobic interaction, and on the contrary the imprinted factors enhanced in the whole concentration range, as shown in Fig. 8B. Previous SMZ-imprinted adsorbents could only get relatively good recognition ability in organic solvent, but poor in pure water system. Through surface grafting of hydrophilic polymer without blocking effective imprinted sites, this novel imprinted nanoadsorbent exhibited good selective recognition for template SMZ in water medium.

Langmuir and Freundlich isotherm models [42] are used to analyze adsorption experimental data, the non-linear forms of which are listed as following equations (3) and (4), respectively:

$$Q_e = \frac{K_L Q_m C_e}{1 + K_L C_e} \tag{3}$$

$$Q_e = K_F C_e^{1/n} \tag{4}$$

where Q_m (μmol g^{-1}) represents the maximum monolayer adsorption capacity. K_L (L μmol^{-1}) and K_F ((μmol g^{-1})(L μmol^{-1})$^{1/n}$) represent Langmuir and Freundlich constant, respectively.

Fig. 9 shows the non-linear fitting curves of adsorption isotherm for MMINs, MNINs, HMNINs and HMNINs towards SMZ, and the isotherm constants are listed in table 1. From Fig. 9, Langmuir fitting curves were deviated from the experimental data for all the four nanoadsorbents. However, the fitting correlation coefficients (R^2) of Freundlich model for the four nanoadsorbents were all higher than 0.997, exhibiting the good correlations, Meanwhile, the fitting curves of Freundlich isotherm agreed well with the experimental data. The *n* values were all higher than 1.0, suggesting the procedure was in favor of SMZ adsorption. Thus, the Freundlich model could better describe the adsorption data, and multi-molecular layer adsorption was dominant in the adsorption process.

3.4. Adsorption kinetics

Batch adsorption experiments were performed to investigate kinetic property of MMINs, MNINs, HMMINs and HMNINs. The kinetic curves of four nanoadsorbents are shown in Fig. 10. In the initial stage, owing to the existence of large empty binding sites, adsorption amount quickly increased. With the increase of contact time, effective binding sites were gradually captured, and adsorption amount slowly achieved equilibrium. Due to the ultrathin polymer film, the adsorption

equilibrium time was very short, which of MMINs, MNINs, HMMINs and HMNINs was only 60 45, 45, and 30 min, respectively. Obviously, after grafting of PHEMA brushes, the adsorption equilibrium time was shorter, might be caused by the improvement of surface hydrophilicity and the increase of the contact probability in water. Also, the adsorption amounts of MMINs and HMMINs were higher than that of the correspondent MNINs and HMNINs in the whole time range.

In order to study adsorption kinetics, the pseudo-first-order and pseudo-second-order kinetic equations [43] are commonly used to analyze the kinetics data, the linear forms of which are shown as following equations (5) and (6), respectively:

$$\ln(Q_e - Q_t) = \ln Q_e - k_1 t \quad (5)$$

$$\frac{t}{Q_t} = \frac{1}{k_2 Q_e^2} + \frac{t}{Q_e} \quad (6)$$

where k_1 (min^{-1}) and k_2 (g μmol^{-1} min^{-1}) represent the pseudo-first-order and pseudo-second-order kinetic constants, respectively.

The linear fitting curves of adsorption kinetics for MMINs, MNINs, HMNINs and HMNINs toward SMZ are shown in Fig. 11 and the kinetic constants are listed in Table 2. For all the four nanoadsorbents, the R^2 values of pseudo-second-order kinetic equation were higher than that of pseudo-first-order kinetic equation, which were all higher than 0.996, exhibiting good linear correlations. As shown in Table 2. the $Q_{e,c}$ values from the pseudo-second-order kinetic equation are more closer to the experimental values. All the results suggested the adsorption processes were better described by the pseudo-second-order kinetic model. Also, it is obviously seen that k_2 values increased after surface-grafting of the hydrophilic polymer brushes, might be caused by the reduction of binding time between the SMZ molecule and nanoadsorbents.

3.5. Selective adsorption ability

In this section, CIP and TC were selected as reference antibiotics to investigate the specific adsorption performance of selective nanoadsorbents. The initial concentration of each antibiotic was 100 μmol L^{-1}, and the process was carried out at 25 ^{o}C for 12 h to reach adsorption equilibrium. The adsorption capacities of HMMINs and HMNINs toward three antibiotics are shown in Fig. 12. Adsorption amounts of HMNINs toward SMZ, TC and CIP were 12.6± 0.567,

17.24±0.64 and 11.42±0.52μmol g^{-1}, respectively, showing no specific recognition. Meanwhile, the HMMINs had a larger adsorption amount of SMZ (33.44±1.22 μmol g^{-1}) than that of TC (19.77±0.78 μmol g^{-1}) and CIP (15.63±0.63 μmol g^{-1}), respectively. Adsorption amounts of TC and CIP onto HMMINs and HMNINs had a little difference. However, adsorption amount of HMMINs was very larger than that of HMNINs toward SMZ. The phenomenon could be explained that HMMINs had the imprinted recognition sites in the polymer network, which matched with molecule size, space structure and functional groups of SMZ template. There were no imprinted sites in the HMNINs, thus showing no selective ability. The above results demonstrated that the imprinted nanoadsorbents were successfully synthesized and the specific recognition ability was satisfying.

3.6. Regeneration performance of HMMINs

The regeneration ability is one of key factors for application performance of adsorbents. Batch adsorption experiment for HMMINs was first conducted to reach saturation adsorption. The SMZ adsorbed onto HMMINs was completely eluted by the mixture solvent of methanol and acetic acid (v:v=9:1). The adsorption-desorption cycles were carried out to test the reuse ability of HMMINs, and the experimental results are shown in Fig. 13. After seven cycles, the adsorption amount of HMMINs toward SMZ in aqueous solution had only a reduction of 7.62 %, exhibiting a good stability and regeneration performance.

4. Conclusion

In conclusion, the HMMINs was successfully prepared *via* a two-step surface-initiated ATRP from the surface of MHNTs. Characterization results showed the thickness of imprinted film and hydrophilic polymer brushes was about 12 and 2-4 nm, respectively. HMMINs had a good thermal and chemical stability, and ideal magnetic property. After the surface grafting of hydrophilic polymer brushes, the static water contact angle obviously reduced to 45.14±0.2^{o} with hydrophobic interaction being inhibited. Although adsorption amount decreased, the imprinted factor increased in the whole concentration range. The adsorption isotherm data was well described by Freundlich model. Due to the ultrathin polymer nanofilm, the adsorption process for HMMINs could reach the equilibrium within 45 min, and the kinetics data was better fitted to the pseudo-second-order rate equation. Besides, HMMINs exhibited a good specific recognition to template molecule SMZ

and regeneration performance. This approach not only developed a simple and general synthesis technique for molecularly imprinting in the aqueous system, but also for obtaining the multifunctional (e.g. hydrophilic, thermosensitive and photosensitive) imprinted nanoadsorbents without affecting recognition sites, to achieve highly efficient and selective removal of various pollutions from water.

Acknowledgments

This work was financially supported by the National Natural Science Foundation of China (Nos. 21176107, 21174057, 21277063, 21446015 and U1407123), the National Basic Research Program of China (973 Program, 2012CB821500), Natural Science Foundation of Jiangsu Province (BK20140534), Ph.D. Innovation Programs Foundation of Jiangsu Province (No. CXZZ13_0668), Research Fund for the Doctoral Program of Higher Education of China (20133227110022 and 20133227110010) and Jiangsu Planned Projects for Postdoctoral Research Funds (1102119C).

References

[1] A.U. Rajapaksha, M. Vithanage, M. Ahmad, D.C. Seo, J.S. Cho, S.E. Lee, S.S. Lee, Y.Sik Ok, Enhanced sulfamethazine removal by steam-activated invasive plant-derived biochar, J. Hazard. Mater. 290 (2015) 43–50.

[2] M. Pan, C.K.C. Wong, L.M. Chu, Distribution of antibiotics in wastewater-irrigated soils and their, accumulation in vegetable crops in the pearl river delta, southern china, J. Agric. Food Chem. 62 (2014) 11062–11069.

[3] M. Teixidó, J.J. Pignatello, J.L. Beltrán, M. Granados, J. Peccia, Speciation of the ionizable antibiotic sulfamethazine on black carbon (biochar), Environ. Sci. Technol. 45 (2011) 10020-10027.

[4] H. Chena, B. Gaoa, H. Li, Removal of sulfamethoxazole and ciprofloxacin from aqueous solutions by graphene oxide, J. Hazard. Mater. 282 (2015) 201–207.

[5] A.U. Rajapaksha, M. Vithanage, M. Zhang, M. Ahmad, D. Mohan, S.X. Chang, Y.S. Ok, Pyrolysis condition affected sulfamethazine sorption by tea waste biochars, Bioresour. Technol. 166 (2014) 303–308.

[6] M. Shi, F.Y. Ma, Y.L. Han, X.Y. Zhang, H.B. Yu, Removal of sulfonamide antibiotics by

oriented immobilized laccaseon Fe_3O_4 nanoparticles with natural mediators, J. Hazard. Mater. 279 (2014) 203–211.

[7] R.M.P. Leal, L.R.F. Alleoni, V.L.Tornisielo, J.B. Regitano, Sorption of fluoroquinolones and sulfonamides in 13 Brazilian soils, Chemosphere 92 (2013) 979–985.

[8] R. Schirhagl, Bioapplications for molecularly imprinted polymers, Anal. chem. 86 (2014) 250–261.

[9] J. He, L.X. Song, S. Chen, Y.Y. Li, H.L Wei, D.X. Zhao, K.R. Gu, S.S. Zhang, Novel restricted access materials combined to molecularly imprinted polymers for selective solid-phase extraction of organophosphorus pesticides from honey, Food Chem. 187 (2015) 331–337.

[10] P. Lenain, S. De Saeger, B. Mattiasson, M. Hedström, Affinity sensor based on immobilized molecular imprinted synthetic recognition elements, Biosens. Bioelectron. 69 (2015) 34–39.

[11] N. Li, L. Qi, Y. Shen, J. Qiao, Y. Chen, Novel oligo(ethylene glycol)-based molecularly imprinted magnetic nanoparticles for thermally modulated capture and release of lysozyme, ACS Appl. Mater. Interfaces 6 (2014) 17289–17295.

[12] S. Muratsugu, M. Tada, Molecularly imprinted ru complex catalysts integrated on oxide surfaces, Acc. Chem. Res. 46 (2013) 300–311.

[13] D.S. Wang, D.Y. Xie, W.B. Shi, S.D. Sun, C.S. Zhao, Designing a photoresponsive molecularly imprinted system on a silicon wafer substrate surface, Langmuir 29 (2013) 8311–8319.

[14] C.H. Hu, J. Deng, Y.B. Zhao, L.S. Xia, K.H. Huang, S.Q. Ju, N. Xiao, A novel core-shell magnetic nano-sorbent with surface molecularly imprinted polymer coating for the selective solid phase extraction of dimetridazole, Food Chem. 158 (2014) 366–373.

[15] J.D. Dai, J.S. He, A.T. Xie, L. Gao, J.M. Pan, X. Chen, Z.P. Zhou, X. Wei, Y.S. Yan, Novel Pitaya-Inspired Well-Defined Core-Shell Nanospheres with Ultrathin Surface Imprinted Nanofilm from Magnetic Mesoporous Nanosilica for Highly Efficient Chloramphenicol Removal, Chem. Eng. J. 284 (2016) 812–822.

[16] P. Yuan, D.Y. Tan, F. Annabi-Bergaya, Properties and applications of halloysite nanotubes: recent research advances and future prospects, App. Clay Sci. 112-113 (2015) 75–93.

[17] W.O. Yah, H. Xu, H. Soejima, W. Ma, Y.R. Lvov, A. Takahara, Biomimetic dopamine

derivative for selective polymer modification of halloysite nanotube lumen, J. Am. Chem. Soc. 134 (2012) 12134–12137.

[18] G.S. Machado, K.A.D. de Freitas Castro, F. Wypychb, S. Nakagaki, Immobilization of metalloporphyrins into nanotubes of natural halloysite toward selective catalysts for oxidation reactions, J. Mol. Catal. A: Chem. 283 (2008) 99–107.

[19] H.J. Bai, H.Q. Zhang, Y.K. He, J.D. Liu, B. Zhang, J.T. Wang, Enhanced proton conduction of chitosan membrane enabled by halloysite nanotubes bearing sulfonate polyelectrolyte brushes, J. Memb. Sci. 454 (2014) 220–232.

[20] S.X. Zuo, W.J. Liu, C. Yao, X.Z. Li, Y. Kong, X.H. Liu, H.H Mao, Y.R. Li, Preparation of polyaniline-polypyrrole binary composite nanotube using halloysite as hard-template and its characterization, Chem. Eng. J. 228 (2013) 1092–1097.

[21] H. Hemmatpour, V. Haddadi-Asl, H. Roghani-Mamaqani, Synthesis of pH-sensitive poly (N, N-dimethylaminoethyl methacrylate)-grafted halloysite nanotubes for adsorption and controlled release of DPH and DS drugs, Polymer 65 (2015) 143–153.

[22] J.D. Dai, X. Wei, Z.J. Cao, Z.P. Zhou, P. Yu, J.M. Pan, T.B. Zou, C.X. Li, Y.S. Yan, Highly-controllable imprinted polymer nanoshell at the surface of magnetic halloysite nanotubes for selective recognition and rapid adsorption of tetracycline, RSC Adv. 4 (2014) 7961–7978.

[23] T. Jing, H. Xia, J.W. Niu, Y.S. Zhou, Q. Dai, Q.L. Hao, Y.K. Zhou, S.R. Mei, Determination of trace 2,4-dinitrophenol in surface water samples based on hydrophilic molecularly imprinted polymers/nickel fiber electrode, Biosens. Bioelectron. 26 (2011) 4450–4456.

[24] K.C. Hua, L. Zhang, Z.H. Zhang, Y. Guo, T.Y. Guo, Surface hydrophilic modification with a sugar moiety for a uniform-sized polymer molecularly imprinted for phenobarbital in serum, Acta Biomaterialia 7 (2011) 3086–3093.

[25] Y. Yoshimi, N. Ishii, Improved gate effect enantioselectivity of phenylalanine-imprinted polymers in water by blending crosslinkers, Anal. Chim. Acta 862 (2015) 77–85.

[26] G.Q. Pan, Y. Zhang, Y. Ma, C.X. Li, H.Q. Zhang, Efficient one-Pot synthesis of water-compatible molecularly imprinted polymer microspheres by facile RAFT precipitation polymerization, Angew. Chem. Int. Ed. 50 (2011) 11731–11734.

[27] G.Q. Pan, Y. Zhang, X.Z. Guo, C.X. Li, H.Q. Zhang, An efficient approach to obtaining

water-compatible and stimuli-responsive molecularly imprinted polymers by the facile surface-grafting of functional polymer brushes via RAFT polymerization, Biosens. Bioelectron. 26 (2010) 976–982.

[28] M.X. Yang, Y.Y. Zhang, S. Lin, X.L. Yang, Z.J. Fan, L.X. Yang, X.C. Dong, Preparation of a bifunctional pyrazosulfuron-ethyl imprinted polymer with hydrophilic external layers by reversible addition–fragmentation chain transfer polymerization and its application in the sulfonylurea residue analysis, Talanta 114 (2013) 143–151.

[29] Y.L. Liu, Y.Y. Huang, J.Z. Liu, W.Z. Wang, G.Q. Liu, R. Zhao, Superparamagnetic surface molecularly imprinted nanoparticles for water-soluble pefloxacin mesylate prepared via surface initiated atom transfer radical polymerization and its application in egg sample analysis, J. Chromatogr. A 1246 (2012) 15–21.

[30] J.D. Dai, J.M. Pan, L.C. Xu, X.X. Li, Z.P. Zhou, R.X. Zhang, Y.S. Yan, Preparation of molecularly imprinted nanoparticles with superparamagnetic susceptibility through atom transfer radical emulsion polymerization for the selective recognition of tetracycline from aqueous medium. J. Hazard. Mater. 205-206 (2012) 179-188.

[31] L.J. Fang, S.J. Chen, X.Z. Guo, Y. Zhang, H.Q. Zhang, Azobenzene-containing molecularly imprinted polymer microspheres with photo- and thermoresponsive template binding properties in pure aqueous media by atom transfer radical polymerization, Langmuir 28 (2012) 9767–9777.

[32] Z. Adali-Kaya, B. Tse Sum Bui, A. Falcimaigne-Cordin, K. Haupt, Molecularly Imprinted Polymer Nanomaterials and Nanocomposites: Atom-Transfer Radical Polymerization with Acidic Monomers, Angew. Chem. Int. Ed. 54 (2015) 5192–5195.

[33] C.M. Hui, J. Pietrasik, M. Schmitt, C. Mahoney, J. Choi, M.R. Bockstaller, K. Matyjaszewski, Surface-initiated polymerization as an enabling tool for multifunctional (nano-) engineered hybrid materials, Chem. Mater. 26 (2014) 745–762.

[34] K. Matyjaszewski, Atom transfer radical polymerization (ATRP): current status and future perspectives, Macromolecules 45 (2012) 4015–4039.

[35] J.D. Dai, Y.L. Zou, Z.P. Zhou, X.H. Dai, J.M. Pan, P. Yu, T.B. Zou, Y.S. Yan, C.X. Li, Narrowly dispersed imprinted microspheres with hydrophilic polymer brushes for the selective removal of sulfamethazine, RSC Adv. 4 (2014) 1965–1973.

[36] H. Nakajima, A. Ishihara, Y.J. Sawa, E. Sakuno, 3-(4-methylfuran-3-yl)propan-1-ol: a white-spotted atinkbug (eysarcoris ventralis) repellent produced by an endophyte isolated from green foxtail, J. Agric. Food Chem. 58 (2010) 2882–2885.

[37] P. Yuan, P.D. Southon, Z.W. Liu, M.E.R. Green, J.M. Hook, S.J. Antill, C.J. Kepert, Functionalization of halloysite clay nanotubes by grafting with γ-aminopropyltriethoxysilane, J. Phys. Chem. C 112 (2008) 15742–15751.

[38] J.X. He, S. Wang, G.Z. Fang, H.P. Zhu, Y. Zhang, Molecularly imprinted polymer online solid-phase extraction coupled with high-performance liquid chromatography-UV for the determination of three sulfonamides in pork and chicken, J. Agric. Food Chem. 56 (2008) 2919-2925.

[39] S.C. Lee, F.L. Chuang, Y.L. Tsai, H. Chen. Studies on the preparation and properties of sol-gel molecularly imprinted polymer based on tetraethoxysilane for recognizing sulfonamides, J Polym Res. 17 (2010) 737-744.

[40] M. Valtchev, B. S. Palm, M. Schiller, U.Steinfeld, Development of sulfamethoxazole-imprinted polymers for the selective extraction from waters, J. Hazard. Mater. 170 (2009) 722–728.

[41] R.X. Gao, J.J. Zhang, X.W. He, L.X. Chen, Y.K. Zhang, Selective extraction of sulfonamides from food by use of silica-coated molecularly imprinted polymer nanospheres, Anal. Bioanal. Chem. 398 (2010) 451–461.

[42] S. Ghorai, A. Sarkar, M. Raou, A.B. Panda, H. Schönherr, S. Pal, Enhanced removal of methylene blue and methyl violet dyes from aqueous solution using a nanocomposite of hydrolyzed polyacrylamide grafted xanthan gum and incorporated nanosilica, ACS Appl. Mater. Interfaces 6 (2014) 4766–4777.

[43] H.L. Zhang, X.C. Li, G.H. He, J.J. Zhan, D. Liu, Preparation of magnetic composite hollow microsphere and its adsorption capacity for basic dyes, Ind. Eng. Chem. Res. 52 (2013) 16902–16910.

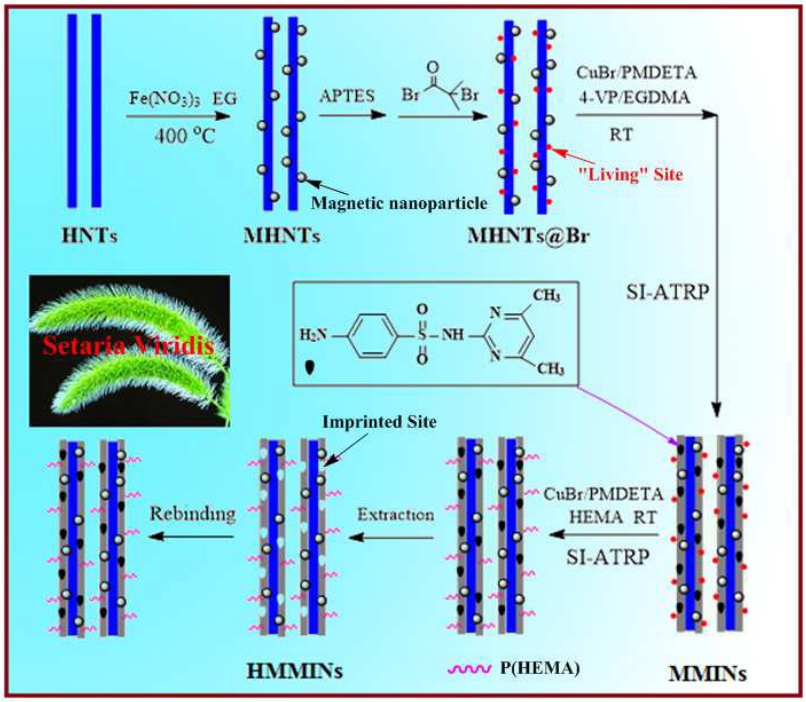

Fig. 1 Schematic diagram of synthetic route for HMMINs.

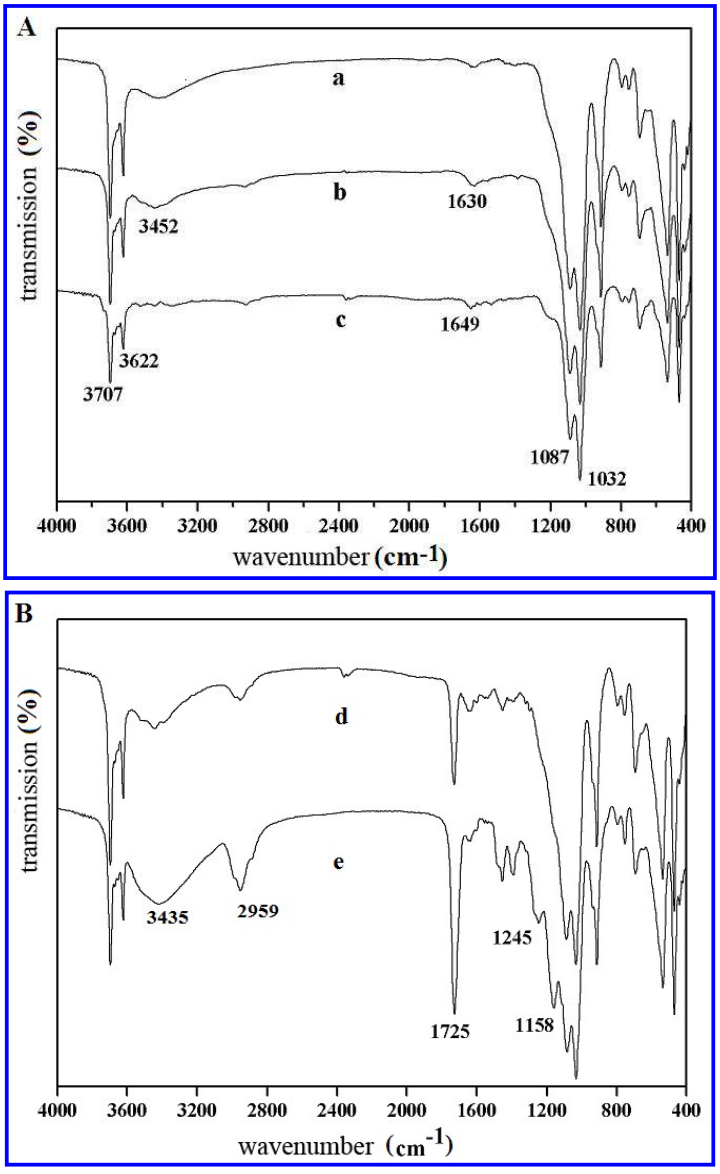

Fig. 2 (A) FT-IR spectra of MHNTs (a), MHNTs@NH_2 (b) and MHNTs@Br (c); (B) MMINs (d) and HMMINs (e).

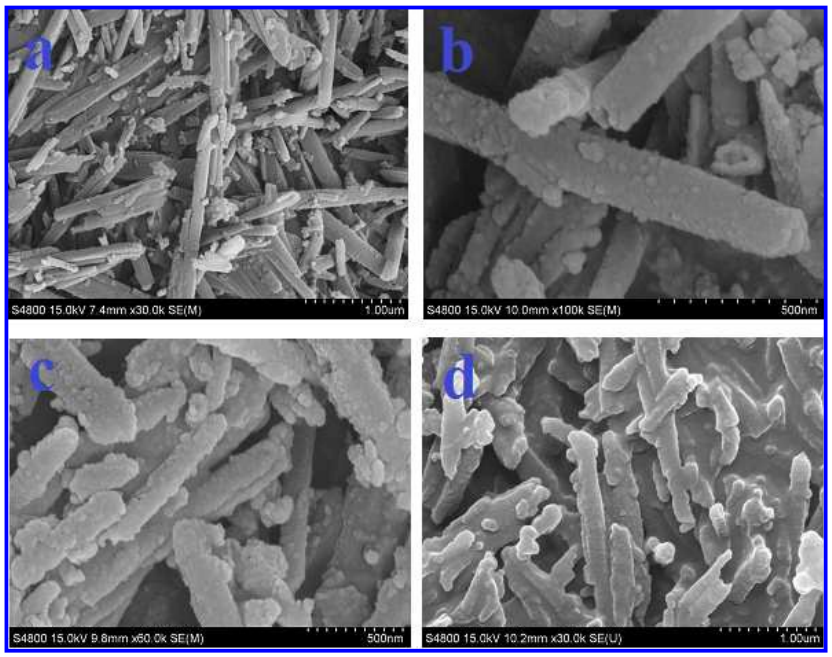

Fig. 3 SEM images of HNTs (a), MHNTs (b), MMINs (c) and HMMINs (d).

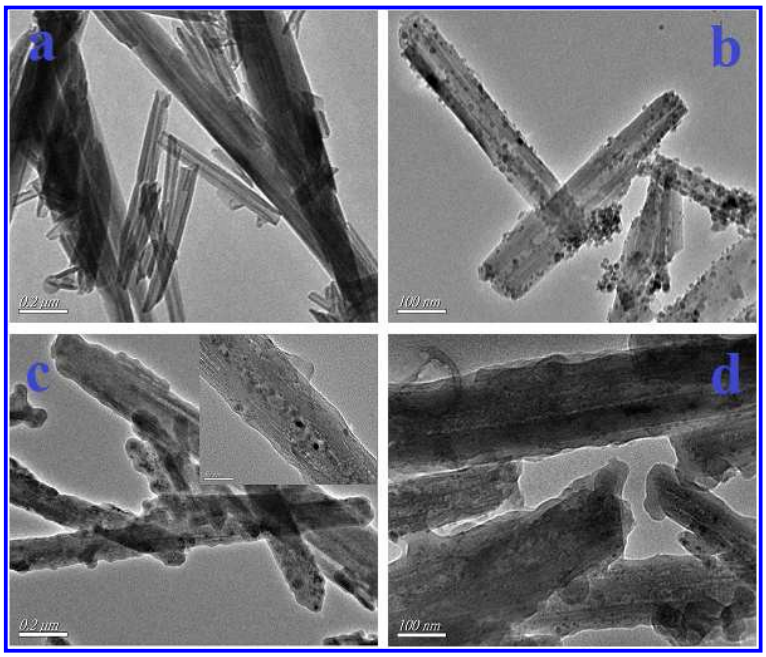

Fig. 4 TEM images of HNTs (a), MHNTs (b), MMINs (c) and HMMINs (d).

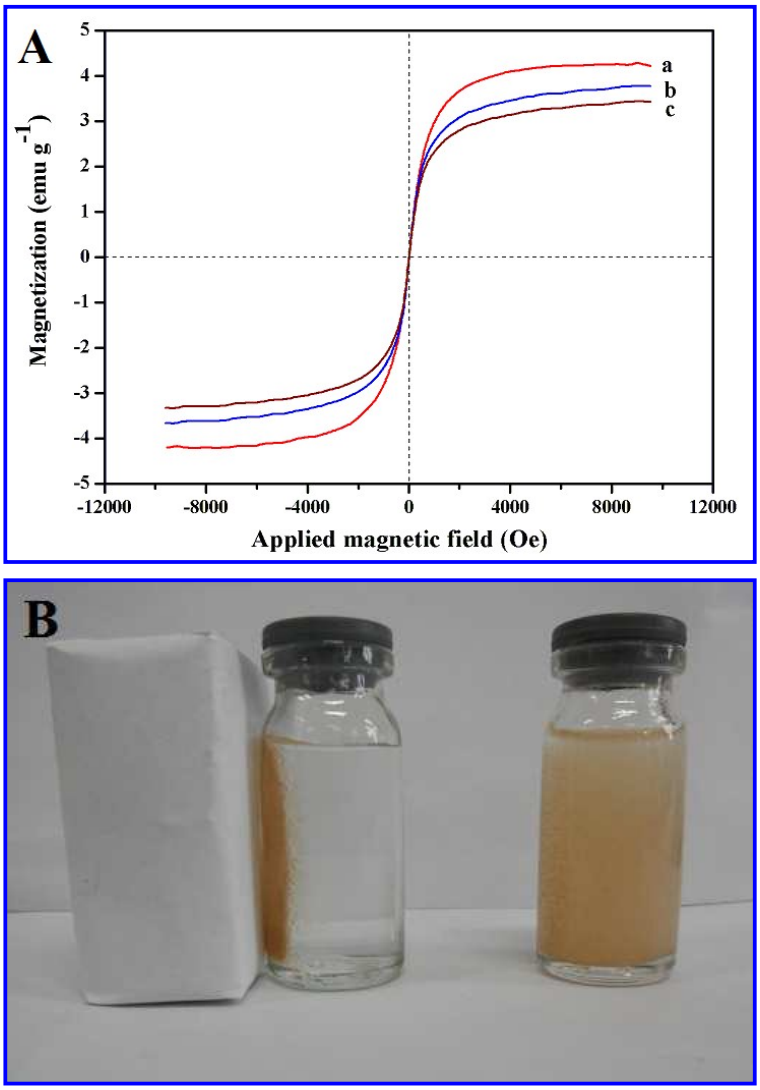

Fig. 5 (A) Magnetization curves of MHNTs (a), MMINs (b) and HMMINs (c) and (B) Photograph of magnetic separation of HMMINs under an external magnet.

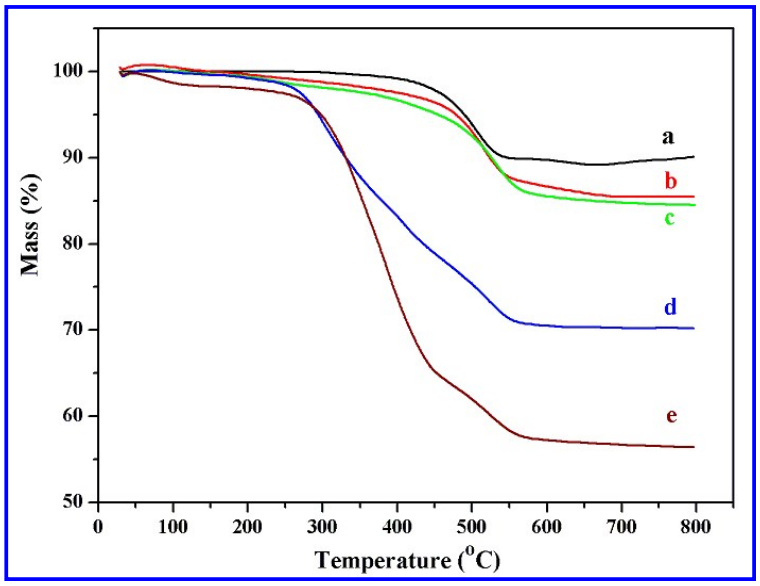

Fig. 6 TGA curves of MHNTs (a), MHNTs@NH_2 (b), MHNTs@Br (c), MMINs (d) and HMMINs (e), respectively.

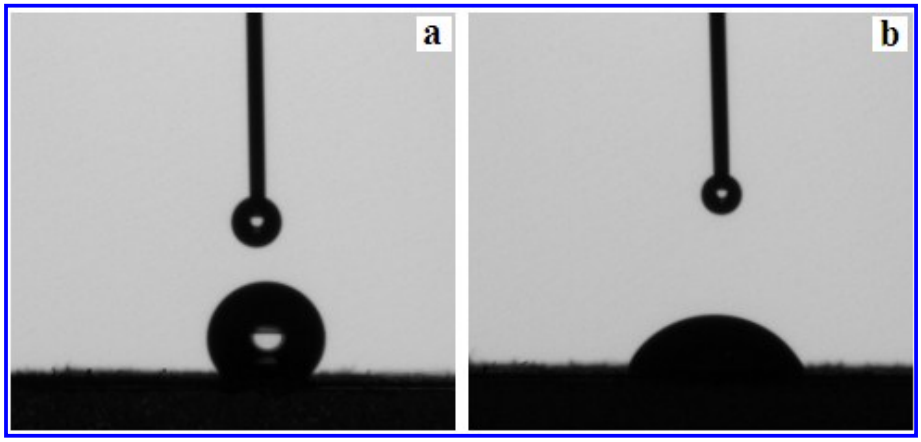

Fig. 7 Photographs of static water contact angle for MMINs (a) and HMMINs (b).

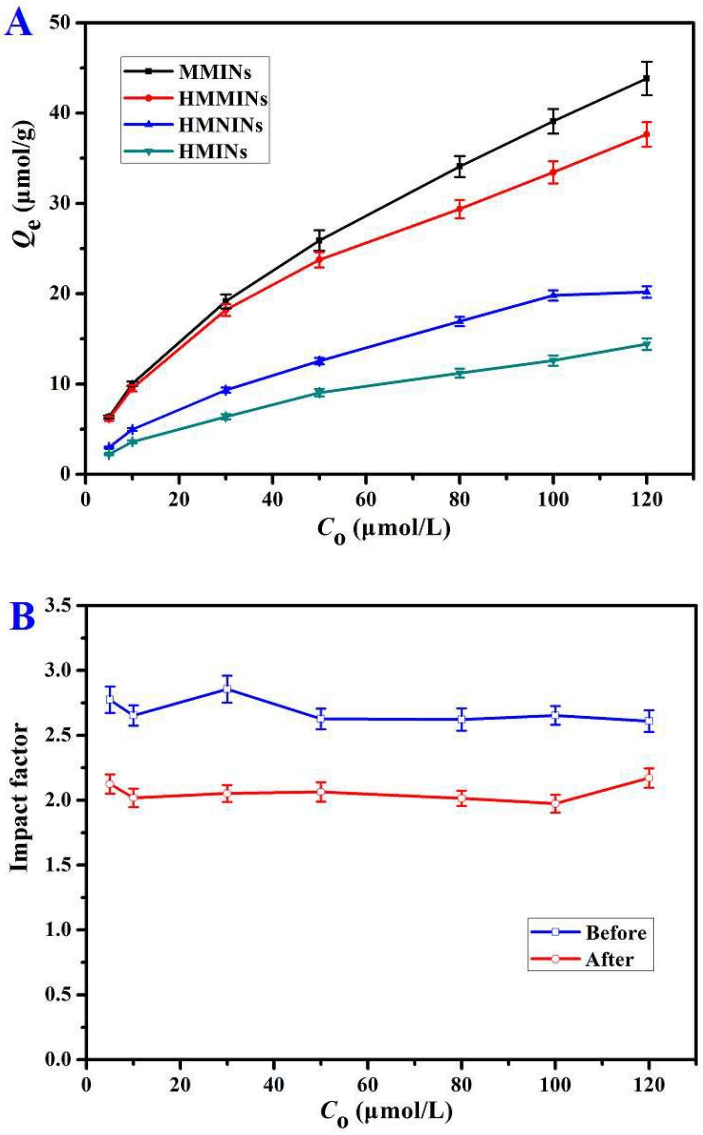

Fig. 8 Adsorption isotherm curves of MMINs, MNINs, HMMINs and HMNINs (a) and imprinted factor before and after surface-grafting (b).

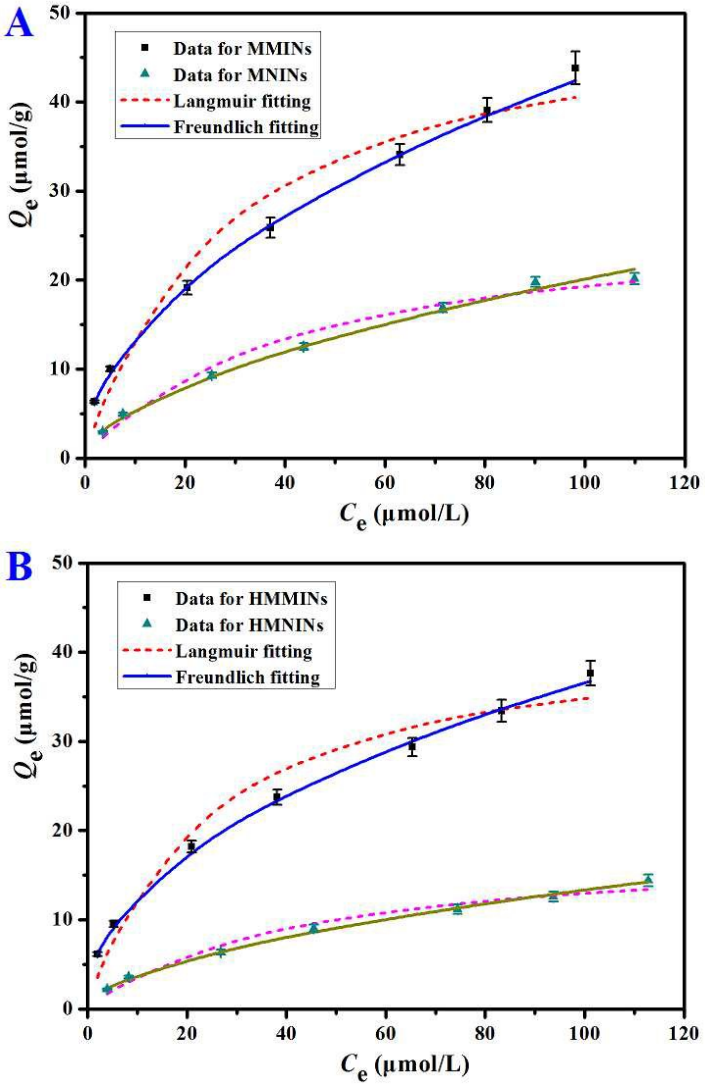

Fig. 9 The non-line fitting curves of Langmuir and Freundlich isotherm for MMINs, MNINs (A), HMNINs and HMNINs (B) toward SMZ at 298 K.

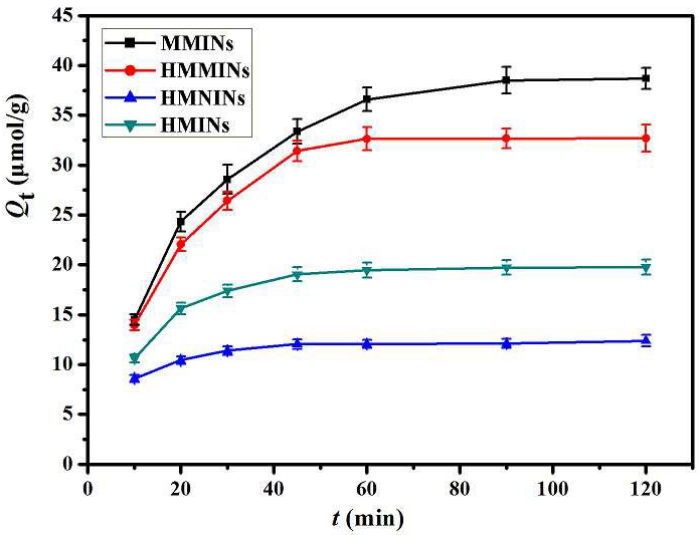

Fig. 10 Adsorption kinetics of SMZ onto MMINs, MNINs, HMNINs and HMNINs at 298 K.

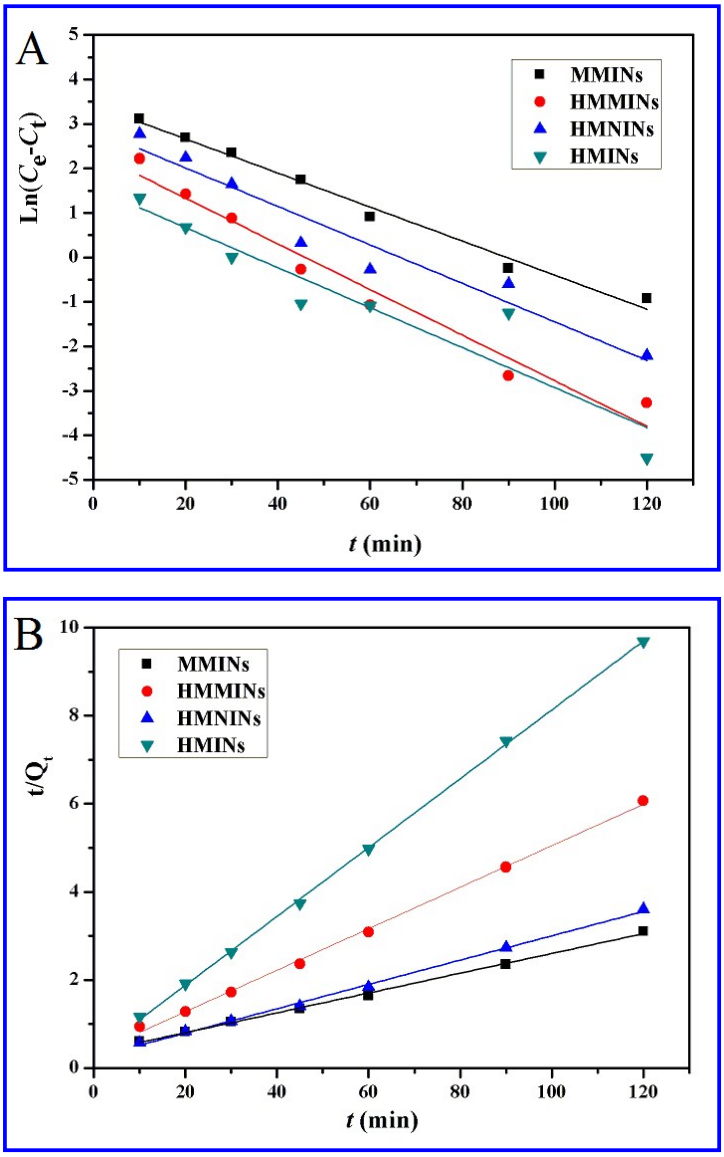

Fig. 11 The linear fitting curves of the pseudo-first-order (A) and pseudo-second-order (B) rate equations for MMINs, MNINs, HMINs and HMNINs toward SMZ.

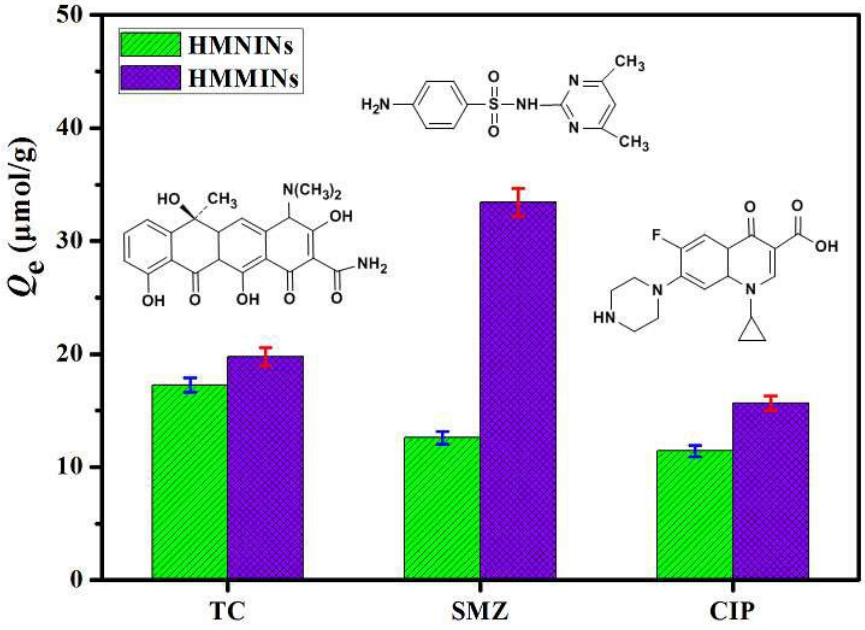

Fig. 12 Chemical structures of three antibiotics (inset) and selective adsorption data of HMMINs and HMNINs.

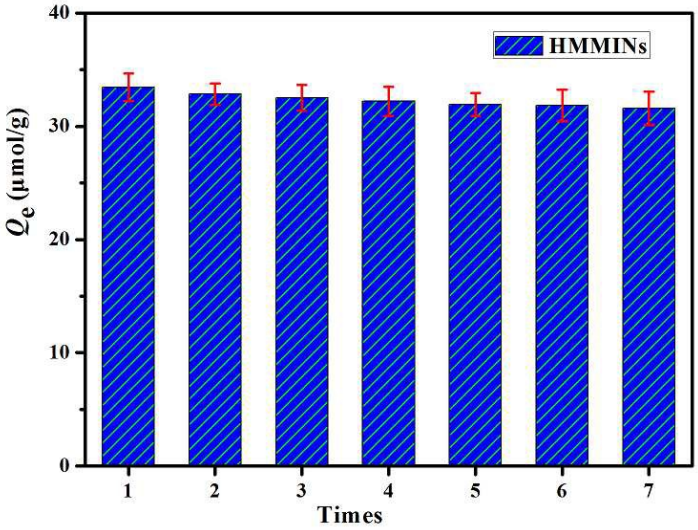

Fig. 13 Regeneration performance of HMMINs toward SMZ.

Table 1

Isotherm constants of MMINs, MNINs, HMMINs and HMNINs toward SMZ at 298 K.

Isotherm models		Langmuir			Freundlich		
Nanoadsorbents	Q_e (μmol g^{-1})	Q_m (μmol g^{-1})	K_L (L mg^{-1})	R^2	K_F (μmol g^{-1}) (L $μmol^{-1})^{1/n}$)	*1/n*	R^2
MMINs	43.82±1.85	50.76	0.04039	0.9461	4.633	0.4829	0.9988
MNINs	20.18±0.625	26.60	0.02664	0.9626	1.535	0.5591	0.9975
HMMINs	37.64±1.36	42.19	0.047239	0.9627	4.561	0.4521	0.9994
HMNINs	14.42±0.649	17.92	0.026399	0.9598	1.721	0.5429	0.9979

Table 2

Adsorption kinetic parameters of pseudo-first-order and pseudo-second-order rate equations of SMZ onto MMINs, MNINs, HMMINs and HMNINs at 298 K.

Kinetic models		Pseudo-first-order			Pseudo-second-order		
Nanoadsorbents	$Q_{e,exp}$ (μmol g^{-1})	$Q_{e,c}$ (μmol g^{-1})	k_1 (min^{-1})	R^2	$Q_{e,c}$ (μmol g^{-1})	k_2 (g μmol $^{-1}$ min^{-1})	R^2
MMINs	39.09±1.36	32.44	0.0386	0.9866	45.25	0.001255	0.9961
MNINs	19.81±0.564	10.55	0.0513	0.9682	21.23	0.006563	0.9981
HMMINs	33.44±1.22	17.73	0.0432	0.9446	37.74	0.003153	0.9977
HMNINs	12.40±0.567	4.791	0.0449	0.8877	12.80	0.019049	0.9996

Biomimetic Setaria Viridis-Inspired Imprinted Nanoadsorbent: Green Synthesis and Application for Highly Selective and Fast Removal of Sulfamethazine

Ping Ma[1], Zhiping Zhou[1,*], Jiangdong Dai[1], Ling Qin[1], Xubo Ye[1], Xiang Chen[2], Jinsong He[2], Atian Xie[2], Yongsheng Yan[2], Chunxiang Li[2,*]

[1] School of Material Science and Engineering, Jiangsu University, Zhenjiang 212013, China

[2] School of Chemistry and Chemical Engineering, Jiangsu University, Zhenjiang 212013, China

Graphical Abstract

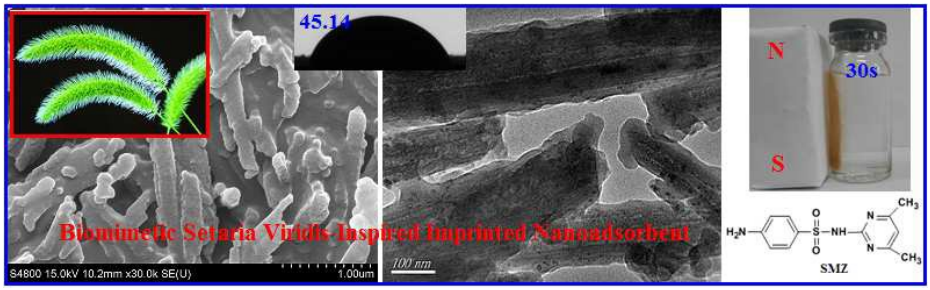

∗ Corresponding author. Tel.: +86-0511-88790683; fax: +86-0511-88791800.

E-mail address: Zhouzp@ujs.edu.cn (Z.P. Zhou); ujs2013txh@163.com (C.X. Li)